Supplementary Information

Structure of a class II preQ$_1$ riboswitch reveals ligand recognition by a new fold

Joseph A. Liberman, Mohammad Salim, Jolanta Krucinska and Joseph E. Wedekind*

Dept. Biochemistry and Biophysics, Center for RNA Biology, University of Rochester School of Medicine and Dentistry, Rochester NY 14642, USA.

*e-mail: joseph.wedekind@rochester.edu

Supplementary Results

Supplementary Table 1 | $PreQ_1$-II Riboswitch Ligand Affinity and Thermodynamic Parameters[a]

	kD	n	ΔH	ΔS	-TΔS	ΔG	ΔΔG[b]
	(nM)		kcal mol^{-1}	kcal K^{-1} mol^{-1}	kcal mol^{-1}	kcal mol^{-1}	kcal mol^{-1}
wild type, 6 mM $MgCl_2$	17.9 ± 0.6	1.00 ± 0.02	-31.9 ± 0.1	-73.4 ± 1.2	21.5 ± 0.1	-10.4 ± 0.1	N/A
MC[c] 6 mM $MgCl_2$	11.6 ± 1.7	1.26 ± 0.17	-32.4 ± 3.7	-74.3 ± 12.9	21.8 ± 0.4	-10.7 ± 0.1	-0.3
C30U[d]	810 ± 120	0.90 ± 0.01	-27.0 ± 0.2	-64.2 ± 1.0	18.8 ± 0.3	-8.2 ± 0.1	2.2
U41C[d]	1600 ± 20	0.83 ± 0.01	-20.5 ± 0.6	-43.3 ± 1.8	12.7 ± 0.5	-7.8 ± 0.1	2.6
wild type, in-line probing condition[e,f]	72.9 ± 0.9	0.85 ± 0.01	-38.2 ± 1.0	-94.6 ± 4.9	28.1 ± 0.9	-10.5 ± 0.4	-0.1
wild type, 0.5 mM EDTA	72.5 ± 6.3	0.57 ± 0.05	-68.6 ± 0.5	-201 ± 1.4	58.9 ± 0.4	-9.7 ± 0.1	0.7
wild type, 1 mM cobalt hexammine	35.6 ± 0.1	1.06 ± 0.02	-27.2 ± 0.3	-58.7 ± 0.9	17.2 ± 0.3	-10.0 ± 0.1	0.4
MC[c] 20 mM $MgCl_2$	10.2 ± 2.6	1.17 ± 0.03	-33.7 ± 1.2	-78.5 ± 4.2	23.0 ± 0.1	-10.7 ± 0.2	-0.3

[a] Thermodynamic parameters are the results mean and standard deviation of two or more independent experiments.

[b] $\Delta\Delta G$ is calculated relative to wild type.

[c] MC is the modified construct (**Supplementary Fig. 1a**) used in crystallization and some ITC analyses.

[d] Mutants were introduced in the context of the wild type sequence (**Fig. 1b**).

[e] In-line probing conditions here were intended to match those used for in-line probing experiments (**Supplementary Fig. 9**). ITC was carried out at 25 °C, with 0.020 M $MgCl_2$, 0.10 M KCl, and 0.050 M HEPPS pH 8.3.

[f] The results indicate a 4-fold loss in $preQ_1$ affinity when the wild type $preQ_1$-II riboswitch 77-mer (**Fig. 1b**) is analyzed under in-line probing conditions (i.e. K_{rel} of 72.9 / 17.9); the change of $MgCl_2$ from 6 mM to 20 mM had no tangible effect on $preQ_1$ binding for MC (**Supplementary Table 1**). The remaining ~4-fold difference in the ITC K_D for $preQ_1$ affinity compared to that obtained from in-line probing (**Supplementary Fig. 9b**; i.e. K_{rel} of ~300 / 72.9) is likely to be the result of differences in the respective constructs (i.e. the 77-mer in **Fig. 1b** versus the extended in-line probing construct in **Supplementary Fig 1b**). This difference is consistent with prior work in which 3.5-fold difference was observed between K_D values measured for the same riboswitch but with different expression platform lengths (summarized in ref. 1).

Supplementary Table 2 | $PreQ_1$-II riboswitch X-ray diffraction and refinement statistics

	SAD Phasing	High Resolution
Data collection		
Space group	$C222_1$	$C222_1$
Cell dimensions		
a, *b*, *c* (Å)	58.1, 86.7, 98.1	58.0, 85.9, 98.1
α, β, γ (°)	α = β = γ = 90°	α = β = γ = 90°
Resolution (Å)	50.0 – 2.6 (2.7 – 2.6) *	25.7 – 2.3 (2.4 – 2.3) *
R_{sym} (%)	8.0 (40.0)	5.3 (23.7)
I / σI	35.2 (9.6)	14.1 (3.0)
Completeness (%)	99.0 (95.8)	97.8 (85.5)
Redundancy	18.1 (18.2)	4.2 (3.8)
Refinement		
Resolution (Å)	50.0 – 2.6	25.7 – 2.3
No. reflections	261,080	47,509
R_{work} / R_{free} (%)	19.4 / 25.1	19.3 / 24.4
No. atoms		
RNA	1571	1612
Ligand	13	13
Cs^+	15	15
Mg^{2+}	5	4
Water	39	152
B-factors (Å^2)		
RNA	35	31
Ligand/ions	35	30
Water	31	28
R.m.s. deviations		
Bond lengths (Å)	0.010	0.008
Bond angles (°)	1.69	1.33

*Values in parentheses represent those for the highest-resolution shell.

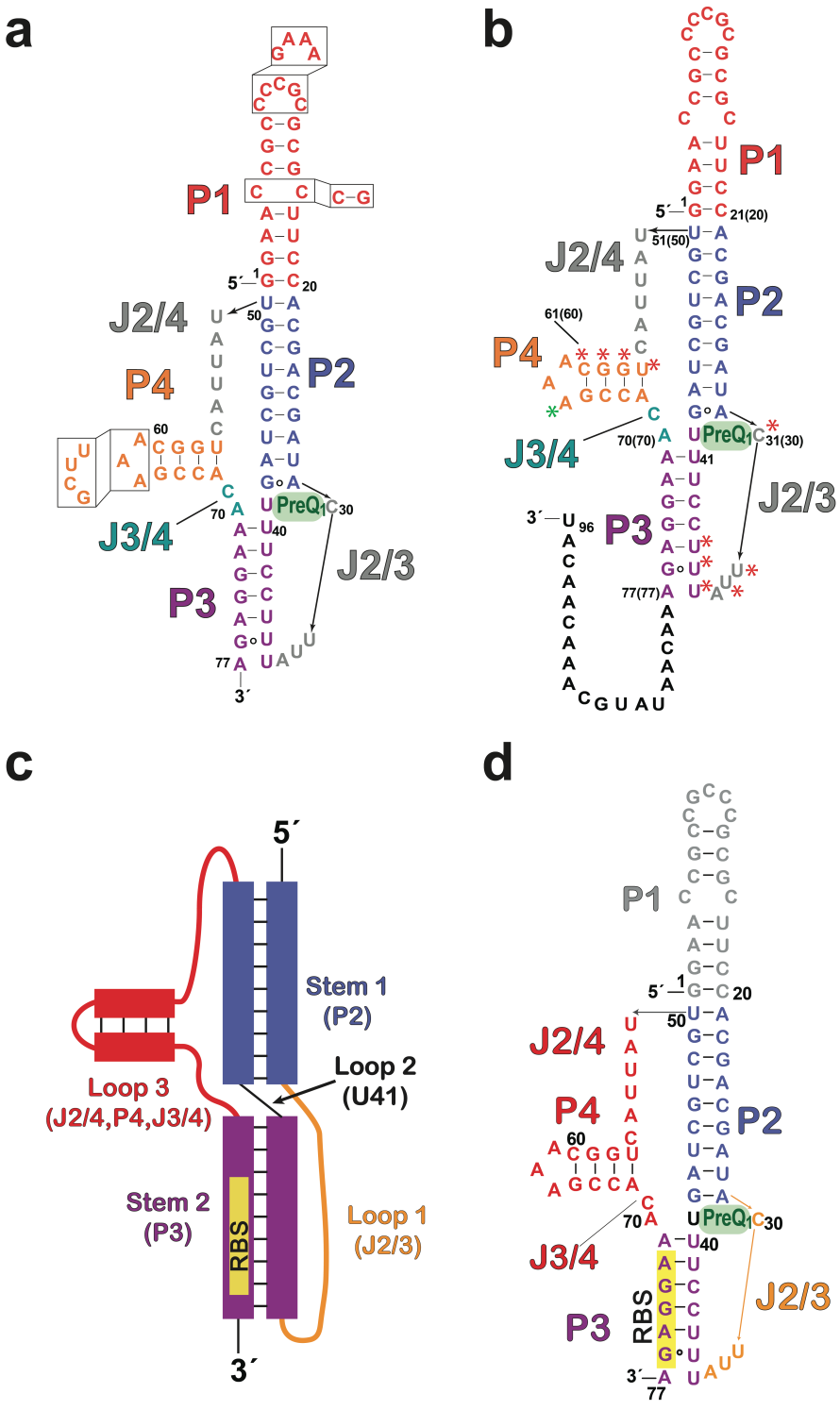

Supplementary Figure 1 | *Lactobacillus rhamnosus* preQ$_1$-II sequences used in this investigation, and pseudoknot classification. (**a**) Changes to wild type (77-mer) sequence that produced the modified construct (MC) for crystallization or ITC are indicated by inset boxes. Areas targeted for changes exhibited low sequence conservation, or dispensability in preQ$_1$

binding[2]. (**b**) The extended wild type (96-mer) sequence used herein for in-line probing. The AUG start codon at the 3´-end was included in addition to the ensuing three codons. The primary numbering is based on the actual wild type sequence; parenthetical values are those from the MC used in crystallization and ITC (i.e. panel **a**); the MC numbering has been adopted throughout the document. Positions analyzed by in-line probing analysis (**Supplementary Fig. 9b**) are marked by asterisks, where red indicates decreased cleavage and green represents increased cleavage as a function of increased $preQ_1$ concentration; see **Supplemental Fig. 9** for experimental results. (**c**) Schematic diagram of an H-type pseudoknot in relation to the $preQ_1$-II riboswitch of this investigation. In the classical definition, stem 1 (equivalent to P2) is followed by loop 1 (equivalent to J2/3), which pairs with loop 3 (J2/4, P4, and J3/4) to form a second helix called stem 2 (P3) (as reviewed in 3). A main difference in topology between the canonical H-type pseudoknot and that of the $preQ_1$-II riboswitch is the extra stem (P4) in the latter. (**d**) Secondary structure of the wild type *L. rhamnosus* $preQ_1$-II riboswitch with bases colored to match the H-type pseudoknot diagram in panel **c**.

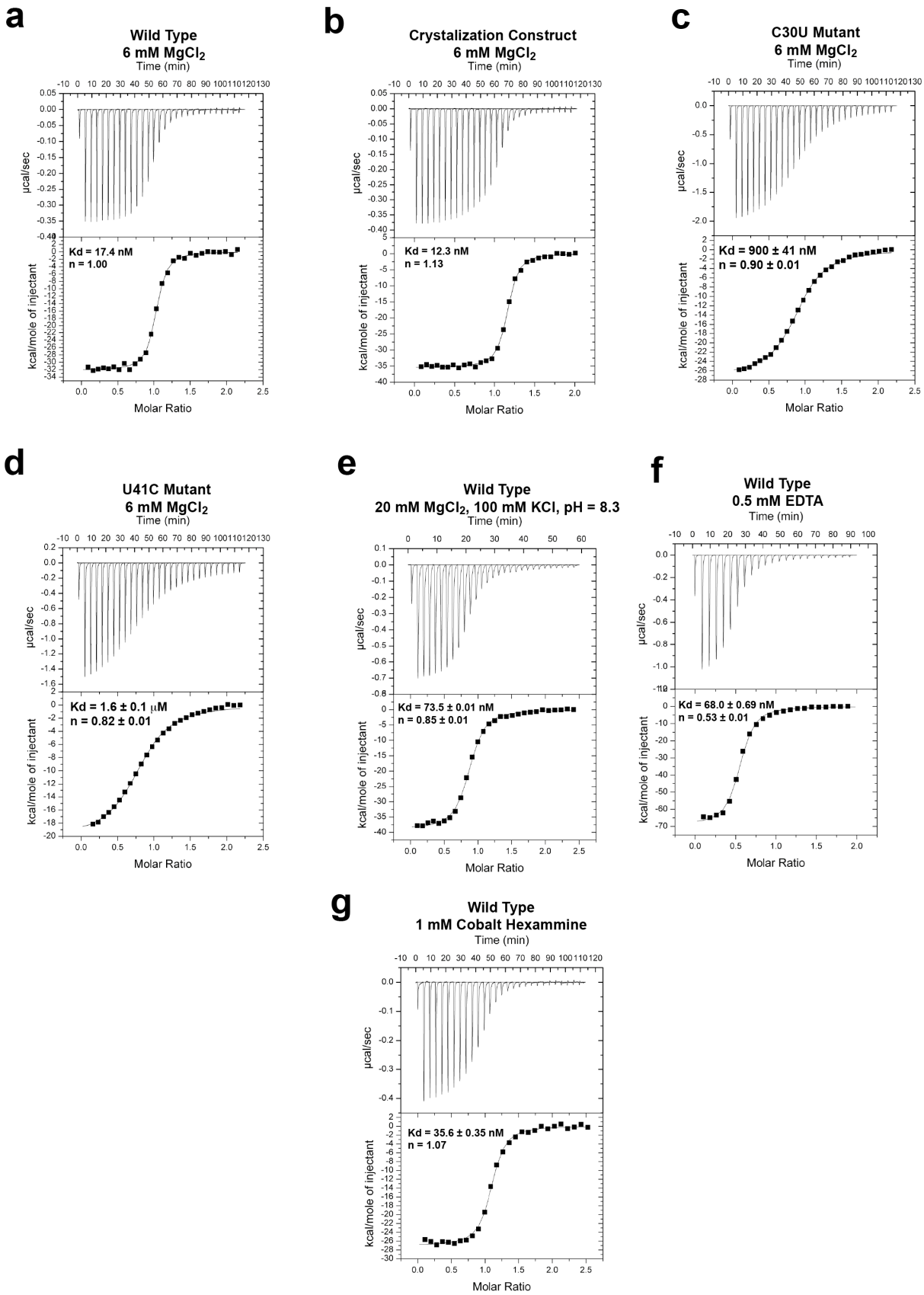
a
Wild Type
6 mM MgCl2
Time (min)
µcal/sec
Kd = 17.4 nM
n = 1.00
kcal/mole of injectant
Molar Ratio
b
Crystalization Construct
6 mM MgCl2
Time (min)
µcal/sec
Kd = 12.3 nM
n = 1.13
kcal/mole of injectant
Molar Ratio
c
C30U Mutant
6 mM MgCl2
Time (min)
µcal/sec
Kd = 900 ± 41 nM
n = 0.90 ± 0.01
kcal/mole of injectant
Molar Ratio
d
U41C Mutant
6 mM MgCl2
Time (min)
µcal/sec
Kd = 1.6 ± 0.1 µM
n = 0.82 ± 0.01
kcal/mole of injectant
Molar Ratio
e
Wild Type
20 mM MgCl2, 100 mM KCl, pH = 8.3
Time (min)
µcal/sec
Kd = 73.5 ± 0.01 nM
n = 0.85 ± 0.01
kcal/mole of injectant
Molar Ratio
f
Wild Type
0.5 mM EDTA
Time (min)
µcal/sec
Kd = 68.0 ± 0.69 nM
n = 0.53 ± 0.01
kcal/mole of injectant
Molar Ratio
g
Wild Type
1 mM Cobalt Hexammine
Time (min)
µcal/sec
Kd = 35.6 ± 0.35 nM
n = 1.07
kcal/mole of injectant
Molar Ratio

Supplementary Figure 2 | Representative isothermal titration calorimetry (ITC) experiments for preQ$_1$ binding to the *L. rhamnosus* preQ$_1$-II riboswitch. Apparent K_D and stoichiometry values (n) for individual experiments are shown; average values are provided in **Supplementary Table 1**. (**a**) PreQ$_1$ binding to the wild type preQ$_1$-II riboswitch (**Fig. 1b** of the main text) in 0.10 M NaCl, 0.006 M $MgCl_2$, and 0.050 M HEPES pH 7.0 (**b**) PreQ$_1$ binding to the MC (**Supplementary Fig. 1a**) under conditions identical to those in **a**. (**c**) PreQ$_1$ binding to the C30U mutant in the context of the wild type *L. rhamnosus* riboswitch sequence under conditions identical to those in **a**. (**d**) PreQ$_1$ binding to the U41C mutant *L. rhamnosus* riboswitch in the context of the wild type *L. rhamnosus* riboswitch sequence under conditions identical to those in panel **a**. (**e**) PreQ$_1$ binding at 25 °C to the wild type riboswitch in 0.10 M KCl, 0.020 M $MgCl_2$, and 0.050 M HEPPS pH 8.3. These conditions are similar to those used for in-line probing (**Supplementary Fig. 9**). (**f**) PreQ$_1$ binding to the wild type riboswitch in 0.10 M NaCl, 0.5 mM EDTA, and 0.050 M HEPES pH 7.0. (**g**) PreQ$_1$ binding to the wild type riboswitch in 0.10 M NaCl, 0.001 M hexammine cobalt(III) chloride, and 0.050 M HEPES pH 7.0.

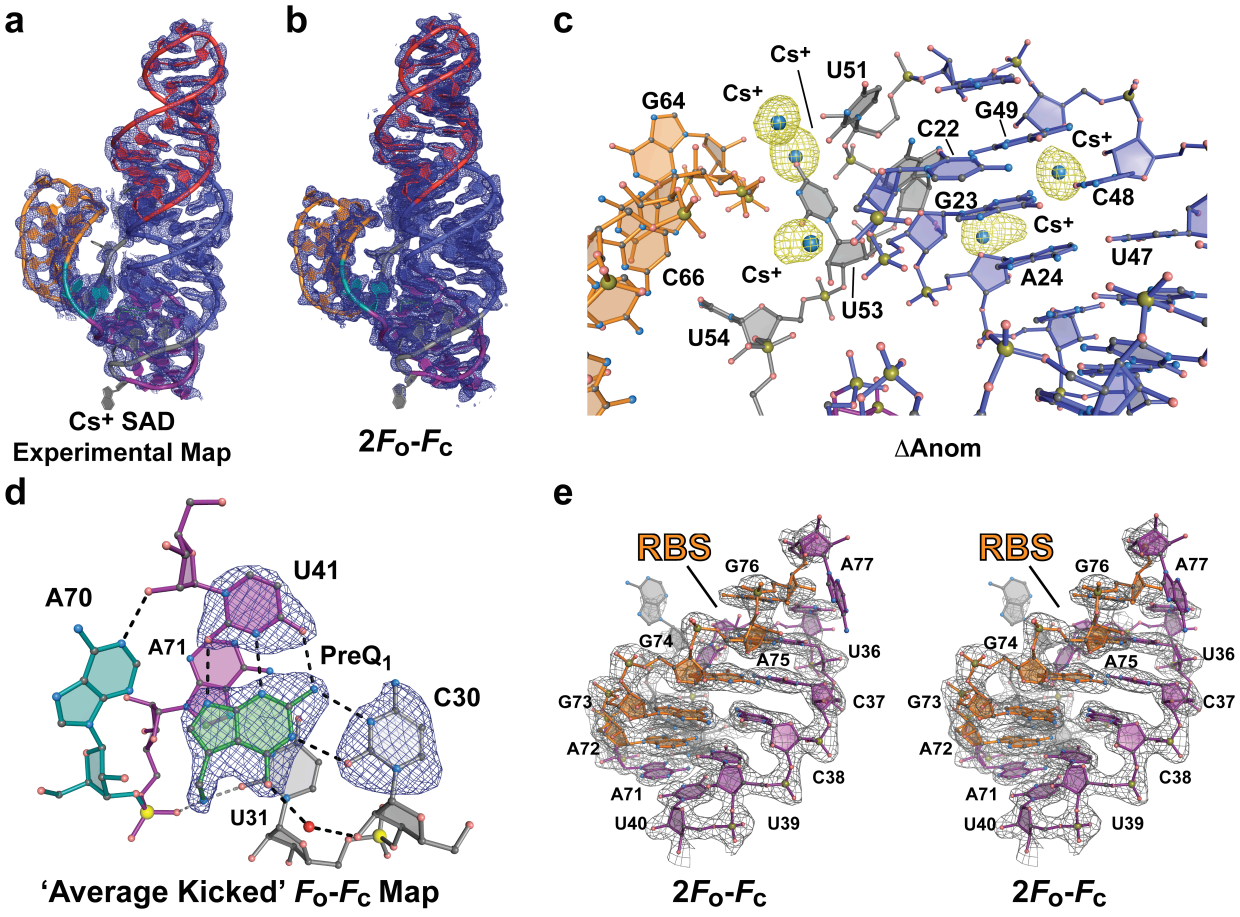

Supplementary Figure 3 | Representative electron-density maps of the preQ$_1$-II riboswitch in the ligand-bound state. (**a**) The 2.6 Å resolution experimental electron density map at the 1.0 σ level was generated by use of the initial density-modified, Cs$^+$-SAD phases; a cartoon from the final refined coordinates is included as in **Fig. 1c**. (**b**) Final 2.3 Å resolution $2F_o - F_c$ electron density at the 1.0 σ level calculated using phases from the final refined model. Bases 33, 34, and 35 of J2/4, as well as 76 and 77 exhibited evidence of conformational disorder but were capable of being modeled; for details see **Supplementary Figure 5a-c**. (**c**) Representative site-bound Cs$^+$ ions used for SAD phasing and included in the final refined coordinates; the accompanying anomalous difference Fourier map at 2.6 Å resolution was contoured at the 3.0 σ level. (**d**) Close up view of the preQ$_1$ binding site. The final refined structure is shown within a σ_a-weighted $F_o - F_c$ averaged kicked electron density map at 2.3 Å resolution calculated with the nucelobases C30 and U41 as well as preQ$_1$ omitted from the phase calculation; the contour level is 3.0 σ. (**e**) Close-up stereo view of the ribosome binding site (RBS) (shown in orange) fit into σ_a-weighted $2F_o - F_c$ electron-density map at 2.3 Å resolution and contoured at the 1.0 σ level. The map was calculated using phases from the final refined model.

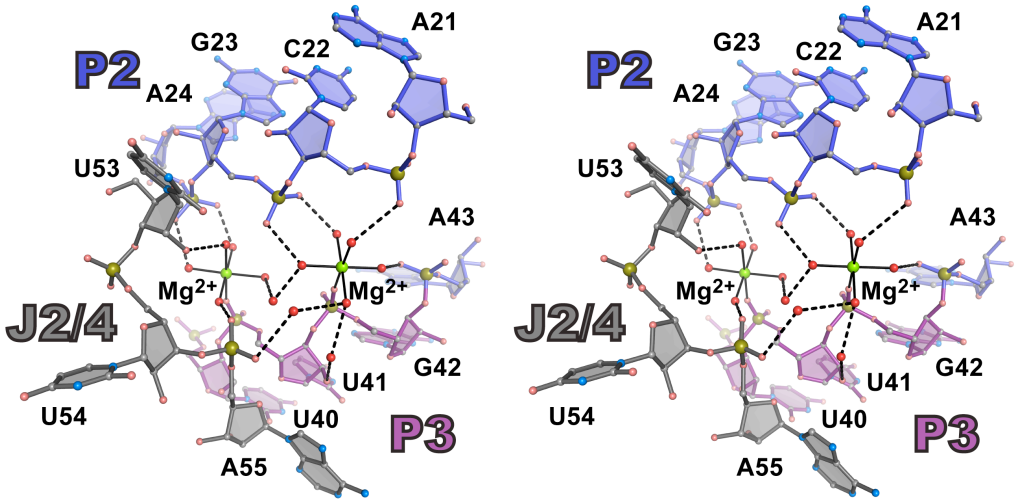

Supplementary Figure 4 | Long-range interactions mediated by site-bound Mg^{2+} ions in the preQ$_1$-II riboswitch. Stereo diagram of the two most prominent Mg^{2+} ions in the structure (depicted in the global view in **Fig. 1c**). One mode of tertiary structure stabilization involves inner and outer sphere contact to RNA and water ligands, which utilizes Mg^{2+} ions with octahedral geometry (as depicted above). ITC experiments performed in the absence of Mg^{2+} (**Supplementary Figure 2f** and **Supplementary Table 1**) demonstrate that the preQ$_1$-II riboswitch can bind ligand in the absence of Mg^{2+}, but is destabilized as indicated by a greater change in entropy upon ligand binding; this observation is similar to Mg^{2+}-free ligand binding by the SAH riboswitch[4]. Moreover, our n value from ITC was ~0.6, indicating a significant fraction of the riboswitch is incompetent to bind ligand in the absence of Mg^{2+}. Furthermore, we observed a modest 2-fold change in ligand binding when $MgCl_2$ is substituted with hexammine cobalt(III) chloride (**Supplementary Figure 2g** and **Supplementary Table 1**), suggesting that multivalent ions can stabilize the riboswitch fold by strictly outer-sphere metal ion contacts.

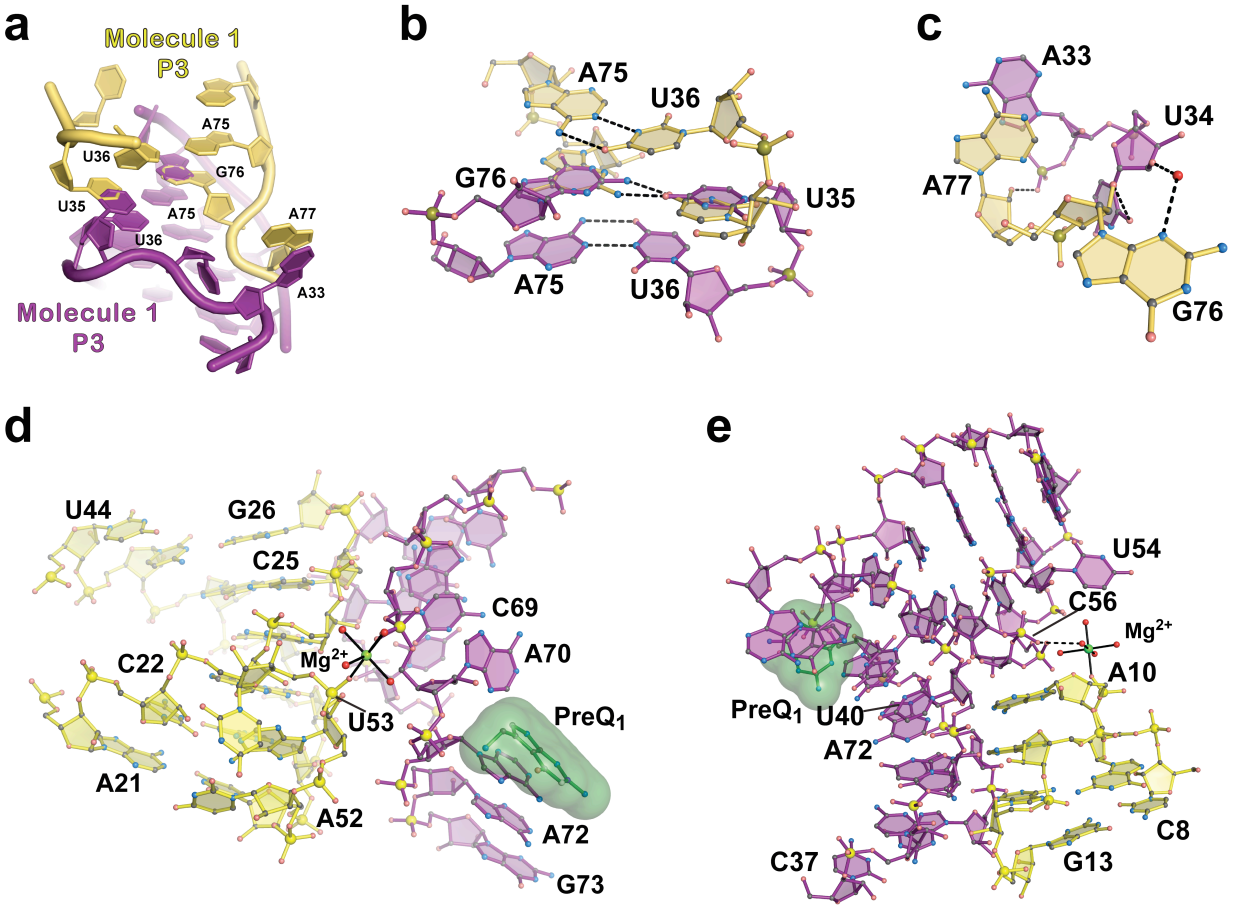

Supplementary Figure 5 | Symmetry-related intermolecular interactions for the preQ$_1$-II riboswitch in the crystal lattice. (**a**) Cartoon showing the 3´-end base stack interaction between P3 of "molecule 1" (purple) and a symmetry related "molecule 1" (yellow). (**b**) Closeup view of the 3´-end from **a** emphasizing the conformational disorder of bases U35 and G76. Here a hydrogen bond forms between N4 of U35 of molecule 1 and N2 of G76 of symmetry-related molecule 2, which is related by a proper dyad axis. Due to the conformational disorder of these bases, each was modeled with 50% occupancy to account for the spatial overlap from symmetry related bases; the remaining 50% occupancy of these positions was assumed to be disordered. (**c**) Close-up of interactions between A77 and G76 of molecule 1, and A33 and U34 of molecule 2 illustrating the chemical sensibility of the long-range interaction, and the unstacking of base A77 from the preceding RBS. (**d**) Close-up view of the preQ$_1$-binding site in which Mg^{2+} (green sphere) mediates inner-sphere contacts between symmetry-related molecules. Significantly, there are no crystal contacts in the immediate vicinity of the ligand. (**e**) Close-up views of two crystal-contact points mediated by inner sphere Mg^{2+} coordination involving intermolecularly related phosphate backbones. The ligand-binding site is shown to emphasize the absence of proximal crystal contacts.

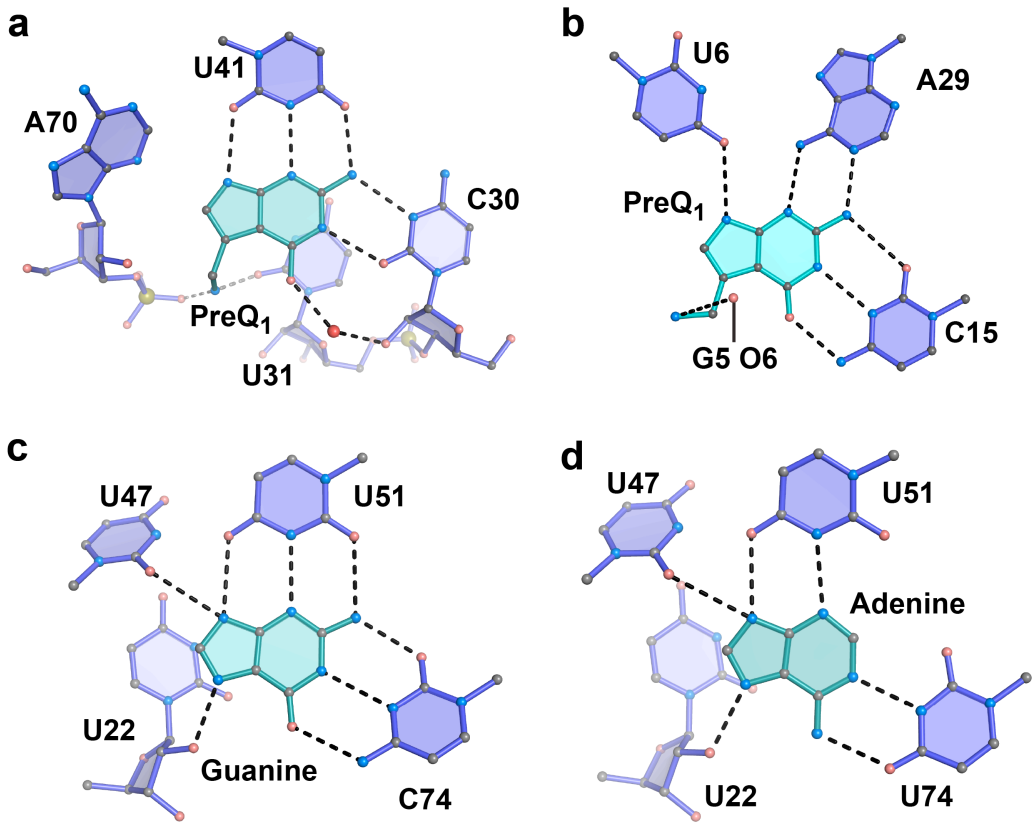

Supplementary Figure 6 | Comparison of ligand recognition by the preQ$_1$-II riboswitch to known riboswitch structures that sense purine-like nucleobase effectors. (**a**) The preQ$_1$-II riboswitch of this investigation in complex with preQ$_1$. (**b**) The preQ$_1$-I translational riboswitch in complex with preQ$_1$ (PDB ID 3Q50)[5]. (**c**) The guanine riboswitch bound to guanine (PDB ID 1Y27)[6]. (**d**) The adenine riboswitch bound to adenine (PDB ID 1Y26)[6].

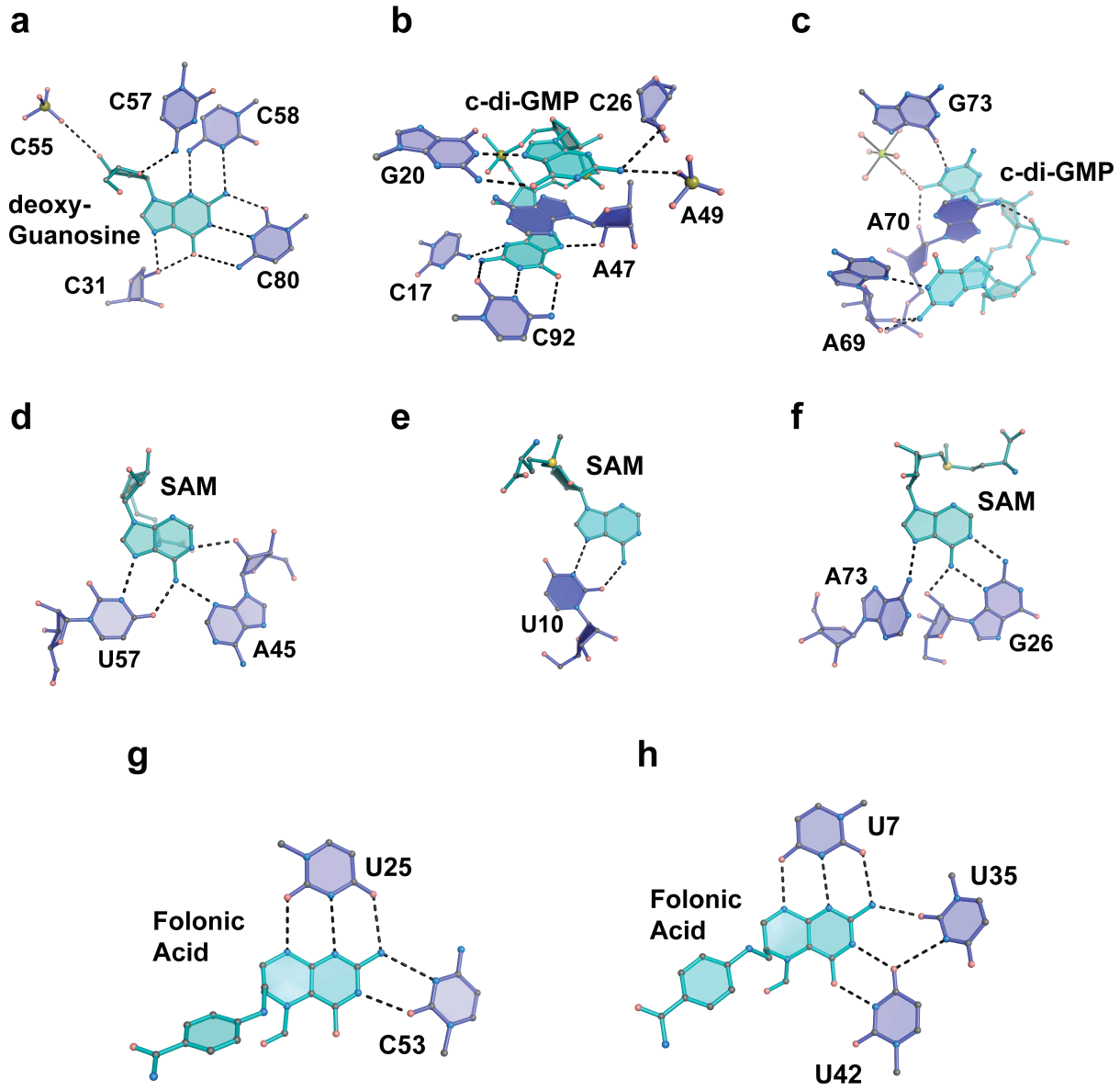

Supplementary Figure 7 | The mode of ligand-recognition by riboswitches that sense effectors containing a purine or purine-like moiety using canonical and non-Watson-Crick pairing. (**a**) The 2´-deoxyguanosine riboswitch bound to its ligand (PDB ID 3SKI)[7]. (**b**) The class I cylic-di-GMP riboswitch bound to the second messenger cyclic-di-GMP (PDB ID 3MXH)[8]. (**c**) The class II cyclic-di-GMP riboswitch bound to cyclic-di-GMP (PDB ID 3Q3Z)[9]. (**d**) The SAM-I riboswitch in bound to S-adenosyl methioine (SAM) (PDB ID 2GIS)[10]. (**e**) The SAM-II riboswitch bound to SAM (PDB ID 2QWY)[11]. (**f**) The SAM-III riboswitch bound to SAM (PDB ID 3E5C)[12]. (**g**) The tetrahydrofolate (THF) riboswitch in complex with folinic acid at the three-way-helical junction binding site (PDB ID 3SD1)[13] appears comparable to the mode of preQ$_1$-II-based readout of preQ$_1$, as described in **Fig. 2a** and **Supplementary Fig. 6a**. (**h**) The THF riboswitch in complex with folinic acid at the pseudoknot binding site (PDB ID 3SD1)[13]. Despite the presence of a trans-Watson-Crick/Watson-Crick pair, the mode of effector recognition by U42 and U35 is relatively dissimilar to interactions employed by C30 of the preQ$_1$-II riboswitch.

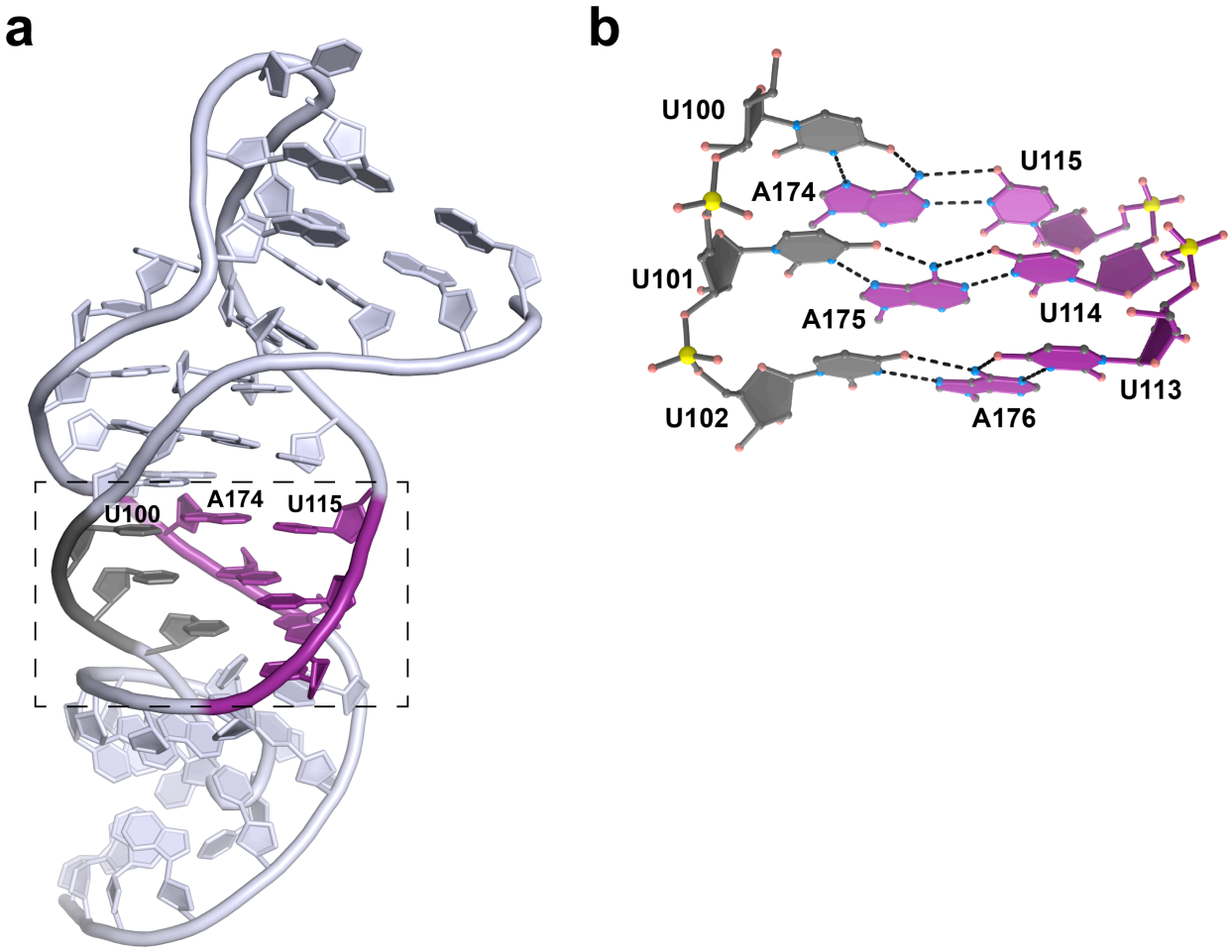

Supplementary Figure 8 | The human telomerase RNA (hTR) pseudoknot structure (PDB ID 1YMO)[14]. (a) Ribbon diagram of the hTR structure depicting the H-type pseudoknot. The bases that compose the hTR major-groove base triples are colored using the same scheme as those that form the major-groove base triples flanking the pseudoknot in the preQ$_1$-II riboswitch (**Fig. 2d**). (**b**) Expanded view of the base triples from hTR including: U100•A174-U115, U101•A175-U114, and U102•A176-U113; these position are spatially comparable to: C30•PreQ$_1$•U41, U31•A71-U40, and U32•A72-U39, respectively, shown in **Fig. 2e**.

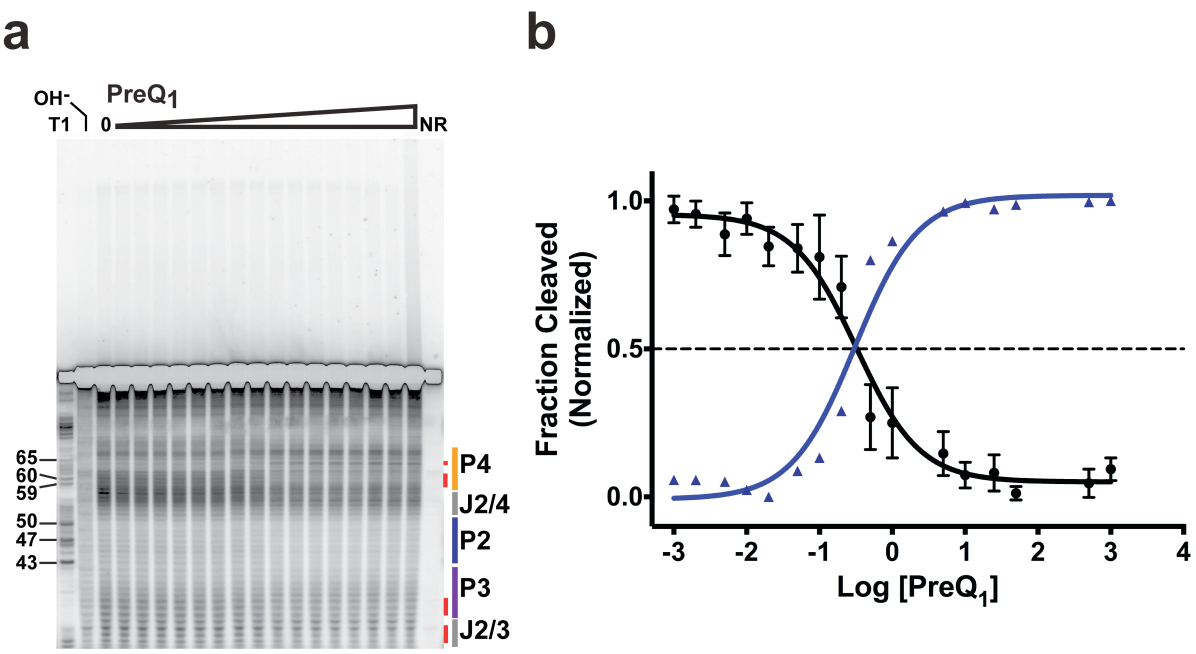

Supplementary Figure 9 | Representative in-line probing gel of the wild type *L. rhamnosus* preQ$_1$-II riboswitch. (**a**) Denaturing polyacrylamide gel depicting in-line probing results conducted on the wild type preQ$_1$-II riboswitch sequence (**Supplementary Fig. 1b**). From left to right, the preQ$_1$-II riboswitch was incubated in the presence of increasing preQ$_1$ at the following concentrations: none, 1 nM, 2 nM, 5 nM, 10 nM, 20 nM, 50 nM, 100 nM, 200 nM, 500 nM, 1 μM, 5 μM, 10 μM, 25 μM, 50 μM, 500 μM, and 1000 μM. Nucleotide positions from the T1 digest are labeled on the left side. The alkaline ladder is indicated by OH^-. Regions used in the analysis in **b** are shown by vertical red bars; secondary structure elements are color coded as in **Supplementary Fig. 1b**; and NR indicates no reaction. (**b**) Plot of the mean fraction cleaved and standard deviation at each concentration of preQ$_1$ for bases: 30, 31, 32 of the major-groove base triples; 34, 35, 36 of the anti-RBS; and 57, 58, 59, and 60 of P4 versus log of preQ$_1$ concentration in μM (shown as black circles with a black curve). A separate curve was plotted for position 63 in the stem loop of P4 (shown as blue triangles with a blue line), which exhibits increased flexibility with increasing preQ$_1$, as shown previously[2]. Both curves gave apparent K_D values of 0.3 μM. Positions used in this analysis are marked by asterisks in **Supplementary Fig. 1b**. Numbering is based on the MC scheme in **Supplementary Fig. 1a**.

References

1 Rieder, U., Kreutz, C. & Micura, R. Folding of a transcriptionally acting preQ$_1$ riboswitch. *Proc. Natl. Acad. Sci. USA* **107**, 10804-10809, (2010).

2 Meyer, M. M., Roth, A., Chervin, S. M., Garcia, G. A. & Breaker, R. R. Confirmation of a second natural preQ$_1$ aptamer class in Streptococcaceae bacteria. *RNA* **14**, 685-695, (2008).

3 Liu, B., Mathews, D. H. & Turner, D.H. RNA pseudoknots: folding and finding. *F1000 Reports Biol.* **2**, 8, (2010).

4 Edwards, A. L., Reyes, F. E., Heroux, A. & Batey, R. T. Structural basis for recognition of S-adenosylhomocysteine by riboswitches. *RNA* **16**, 2144-2155, (2010).

5 Jenkins, J. L., Krucinska, J., McCarty, R. M., Bandarian, V. & Wedekind, J. E. Comparison of a preQ$_1$ riboswitch aptamer in metabolite-bound and free states with implications for gene regulation. *J. Biol. Chem.* **286**, 24626-24637, (2011).

6 Serganov, A. *et al.* Structural basis for discriminative regulation of gene expression by adenine- and guanine-sensing mRNAs. *Chem. Biol.* **11**, 1729-1741, (2004).

7 Pikovskaya, O., Polonskaia, A., Patel, D. J. & Serganov, A. Structural principles of nucleoside selectivity in a 2'-deoxyguanosine riboswitch. *Nat. Chem. Biol.* **7**, 748-755, (2011).

8 Smith, K. D., Lipchock, S. V., Livingston, A. L., Shanahan, C. A. & Strobel, S. A. Structural and biochemical determinants of ligand binding by the c-di-GMP riboswitch. *Biochemistry* **49**, 7351-7359, (2010).

9 Smith, K. D., Shanahan, C. A., Moore, E. L., Simon, A. C. & Strobel, S. A. Structural basis of differential ligand recognition by two classes of bis-(3'-5')-cyclic dimeric guanosine monophosphate-binding riboswitches. *Proc. Natl. Acad. Sci. USA* **108**, 7757-7762, (2011).

10 Montange, R. K. & Batey, R. T. Structure of the S-adenosylmethionine riboswitch regulatory mRNA element. *Nature* **441**, 1172-1175, (2006).

11 Gilbert, S. D., Rambo, R. P., Van Tyne, D. & Batey, R. T. Structure of the SAM-II riboswitch bound to S-adenosylmethionine. *Nat. Struct. Mol. Biol.* **15**, 177-182, (2008).

12 Lu, C. *et al.* Crystal structures of the SAM-III/S(MK) riboswitch reveal the SAM-dependent translation inhibition mechanism. *Nat. Struct. Mol. Biol.* **15**, 1076-1083, (2008).

13 Trausch, J. J., Ceres, P., Reyes, F. E. & Batey, R. T. The structure of a tetrahydrofolate-sensing riboswitch reveals two ligand binding sites in a single aptamer. *Structure* **19**, 1413-1423, (2011).

14 Theimer, C. A., Blois, C. A. & Feigon, J. Structure of the human telomerase RNA pseudoknot reveals conserved tertiary interactions essential for function. *Mol. Cell* **17**, (2005).